Master's Thesis

Effect of Filler Particle Characteristics on Yield Stress and Plastic Viscosity of Sulfur Composites

Lee Jin Hyun

Department of Urban and Environmental Engineering

(Urban Infrastructure Engineering)

Graduate School of UNIST

2018

Effect of Filler Particle Characteristics on Yield Stress and Plastic Viscosity of Sulfur Composites

Lee Jin Hyun

Department of Urban and Environmental Engineering
(Urban Infrastructure Engineering)

Graduate School of UNIST

Effect of Filler Particle Characteristics on Yield Stress and Plastic Viscosity of Sulfur Composites

A thesis
submitted to the Graduate School of UNIST
in partial fulfillment of the
requirements for the degree of
Master of Science

Lee Jin Hyun

06. 08. 2018
Approved by

Advisor
Myoungsu Shin

Effect of Filler Particle Characteristics on Yield Stress and Plastic Viscosity of Sulfur Composites

Lee Jin Hyun

This certifies that the thesis of Lee Jin Hyun is approved.

06. 08. 2018

Advisor: Myoungsu Shin

Department of Urban and Environmental Engineering
Ulsan National Institute of Science and Technology
Chairperson

Committee Member: Jaeeun Oh
Department of Urban and Environmental Engineering
Ulsan National Institute of Science and Technology
Committee Member

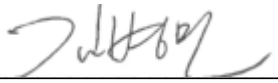

Committee Member: Byungmin Kim
Department of Urban and Environmental Engineering
Ulsan National Institute of Science and Technology
Committee Member

ABSTRACT

Since sulfur has fluidity only at specific temperature (over 115 °C) and it is very sensitive to the temperature, it is necessary to quantitatively evaluate the workability of sulfur concrete. In this study, we considered the sulfur composite as a suspension of filler particles, which are the blends of cement and fly ash, and investigated the influence of filler properties on the rheology of the sulfur composite in paste level, which made of modified sulfur and fillers. The rheological properties of modified sulfur and sulfur composite are measured by parallel plates and the properties of filler particles were measured by laser diffraction. Bingham model to the selected shear strain rate showed better trends of rheological properties of sulfur composite. Yield stress of sulfur composites is mainly affected by the volume fraction of fillers and the type of fillers. Plastic viscosity is mainly affected by the surface area of fillers in sulfur composite. The rheological results and the Krieger-Dougherty model confirmed the intrinsic viscosity in the model equation is affected by the type of binder regardless of their volume fraction in sulfur composite. Consequently, the sulfur composite follows the suspension-rheology models when the proper content of filler was used, which is less than 30% in sulfur composite, and it implies the suspension theories can be applied to the materials based on the sulfur binder.

TABLE OF CONTENTS

LIST OF FIGURES

LIST OF TABLES

CHAPTER 1 – INTRODUCTION

1.1 Research Background

Sulfur is one of the byproducts produced by petroleum refineries and natural gas process plants. There is so much byproduct sulfur that it does not need to be mined anymore, unlike other minerals. However, the demand for the surplus sulfur is very confined, which causes many social and environmental problems. Recently, some part of sulfur begins to be consumed as construction materials, such as building materials and roadway paving, due to its cheap price and unique properties [1]. Sulfur, which is a thermoplastic material, gets a fluidity only at higher temperature (over 115 °C) and gets the strength rapidly during the cooling process. Given that the temperature is controlled, sulfur can replace the cementitious binders in concrete, which is called sulfur concrete [2,3].

Sulfur concrete made of sulfur and aggregates, where the molten sulfur acts like a binder surrounding the aggregates. It produces a rapid strength development, higher ultimate strength, and better resistance to strong acids. While the cement based concrete gets a maximum strength in several weeks at a humid curing condition; it gets about 90 percent of the maximum strength after 28 days, sulfur concrete reaches its maximum strength in a few hours regardless of the humidity condition [4].

When the sulfur is cooled in solid state, its phase is changed from monoclinic sulfur (S_β) to orthorhombic sulfur (S_α). Since sulfur allotropes belong to eight membered ring class, they have different physical properties, molecular structure, and chemical activity. Especially, the phase transition causes the volume reduction and the induced internal stress brings about the shrinkage in sulfur concrete. Due to the shrinkage, sulfur concrete has a critical durability problem such as a repetitive freezing and thawing and continuous exposure to highly humidity condition [2,5].

Modified sulfur can improve the durability problems caused by the shrinkage of elemental sulfur in the process of cooling. Modified sulfur is produced by mixing elemental sulfur and organic chemical additives at 130~150 °C, where the week bonds in ring structure of sulfur are broken and new bonds with the other sulfurs or modifier are formed to make a long chain polymer [1]. Dicyclopentadiene (DCPD) is one of the commonly used modifiers, which plasticizes and stabilize the sulfur in polymeric form. Adding 5 % of DCPD on the composition of sulfur materials keeps the form of orthorhombic sulfur (S_α) and the portion of S_α is dominant [6], which prevents the formation transition and, as the result, reduces the shrinkage problems.

Sulfur cement refers to the mixture of modified sulfur and mineral fillers. Mineral filler improves the workability and strength, allowing the modified sulfur to be used more stably as a binder. Addition of mineral filler controls the viscosity of sulfur cement paste, which affects the workability and reduces segregation between modified sulfur and aggregates. Filler replaces the portion of sulfur, which reduces shrinkage caused by transformation of sulfur during hardening. Fly ash, silicate flour, and crushed dust are the examples of the commonly used mineral fillers [1,7].

Usage of modified sulfur and filler as a binder in concrete induces a better resistance to freezing and thawing due to lower permeability and porosity. After modification, modified sulfur concrete still has advantages such as higher strength, rapid strength development, and a good resistance to most acid or salt condition [1]. Mix design of modified sulfur concrete for construction material considers 4 factors, including a good resistance to acid or salt, lower water absorption, better strength than Portland cement concrete, and enough fluidity for good workability. Many test standards are reported for the performance about mechanical strength and durability such as ASTM C39 [8], ASTM C78 [9], ASTM C496 [10]. On the other hand, there is no standard or recommended test for the workability of sulfur concrete.

In the case of Portland cement concrete, the conventional tests for workability such as slump test have been used for estimating the workability of the concrete. The properties of aggregates and cement influence the workability of Portland cement concrete but the conventional test has a limitation of describing the behavior of flow; it has only one indicator, the value of slump. Due to its insufficiency, many rheological theories have replaced the conventional tests [11]. Rheology, especially rheology for suspension, can describe various flow behaviors and relate the properties of suspended particle (aggregates) and suspending fluid (cement paste) [12]. In case of sulfur concrete, the properties of modified sulfur, filler, and aggregate can influence on the workability of sulfur concrete. Appling the studies for suspension rheology to sulfur concrete will produce better estimation for the performance of sulfur concrete. In this study, the author focuses the effect of the properties of filler to the workability of sulfur composite as the first step for applying rheology to sulfur products.

1.2 Objectives and Scope

In this study, the theory of suspension rheology is applied to sulfur products in paste level and it will be revealed whether rheology can be used to analyze the workability of sulfur products in further studies. The properties of filler particles are characterized by particle size distribution and total surface area of filler. The rheological results will be fitted to the conventional models relating the rheological properties of suspension and the properties of suspended particles, where specific model terms will describe the effect of filler in sulfur composite.

CHAPTER 2 – SUSPENSION RHEOLOGY

2.1 The needs of rheological properties in freshly-mixed normal concrete

In this study, the author focused on the behavior of sulfur in paste level as the first step for evaluating the performance of sulfur concrete. Except for the type of binder, the compositions of normal concrete and sulfur concrete are very similar. Since there are no standards or official tests for the performance of sulfur concrete before hardening, the standards or studies for the freshly mixed normal concrete were examined. One of the intuitive methods to evaluate the fluidity of materials is to visually confirm how much the materials can flow by an external force. For example, the workability of freshly mixed concrete has been evaluated by slump or slump flow test as described in ASTM C143 [13], where the freshly mixed concrete vertically deforms or flows by their self-weight. Based on the test result, the workability, or fluidity, is qualitatively evaluated. This intuitive method is quite simple but it has only one parameter (slump or slump flow) to evaluate the workability of concrete. According to ASTM C143, acceptable ranges of test result for identical test specimens depend on the number of test operator, which implies the intuitive method requires a lot of experience for accurate evaluation [14].

For the exact and quantitative evaluation about the workability of fresh concrete, rheology theory has been studied and applied to the freshly mixed concrete [11,12,14]. In rheology theory, the flow behavior can be described by rheological properties, which obtained by rheometer test and analyzed by some models. Many constitutive model equations have been developed to describe the behavior of freshly mixed concrete. Among them, Bingham model and Herschel-Bulkley model are fitted well with the experimental data [15]. The Bingham model describes the behavior, where the shear stress is linearly proportional to the shear strain rate above some specific shear stress like Eq. (2.1). In terms of the rheological properties, the rate of change for the shear stress to the shear strain rate is defined as plastic viscosity (η) and the minimum shear stress required for the matter to initiate to flow or deform is defined as yield stress (τ_0). Herschel-Bulkley model represents the behavior of materials, where the shear stress has a power growth with increasing shear strain rate above yield stress like Eq. (2.2). In the case of this model, the model constant *a* means the viscosity when the shear rate equals 1 1/s and b is model constant.

$$\tau = \tau_0 + \eta\dot{\gamma} \tag{2.1}$$

$$\tau = \tau_0 + a\dot{\gamma}^b \tag{2.2}$$

2.2 The needs of rheological properties in sulfur concrete before hardening

The difference between normal concrete and sulfur concrete is the type of binder; the sulfur concrete uses modified sulfur in the liquid state instead of cement paste. Mixing cement and water at some ratio produces cement paste with fluidity while melting modified sulfur with high temperature produces modified sulfur in the liquid state. Cement paste has lower flowability as the water-cement ratio is lower and the flowability of modified sulfur is controlled by the temperature and amount of added modifier. Hardening of cement paste occurs due to the hydration react of cement, while modified sulfur gets strength during the cooling. That is, cement is a hydraulic material and modified sulfur is a thermoplastic material [16]. Since the properties of paste influences on that of concrete material, the conventional tests or studies for freshly-mixed normal concrete are needed to be modified, considering the properties of binder materials.

According to the mix design for sulfur concrete proposed by Makenya [17], the sulfur concrete should be designed to find the optimized viscosity of the mixture. Considering the relationship between the sulfur content and mineral filler content, the sulfur concrete with relatively higher sulfur content has a problem such as thermal expansion and abundant microcracking, while the sulfur concrete with lower sulfur content has very poor workability and high porosity. For preventing such defects in sulfur concrete, optimum sulfur content should be found and used. However, the determination of optimum sulfur content requires many experiences and trials. Since sulfur concrete has a workability only with a high temperature and its workability easily varies depending on the temperature, more strict conditions and methods are required to evaluate the workability of sulfur concrete. For example, slump test couldn't be a good indicator for the workability of sulfur concrete because the error from temperature control may additionally affect its original inaccuracy. However, rheology can be applied to evaluate the workability of sulfur concrete without difficulty from the heat condition because some of the rheometers, which are equipment measuring the rheology, can precisely control the temperature of the entire sulfur sample.

Like the rheology studies conducted for normal concrete, the constitutive equations, Bingham or Herschel-Bulkley models, were applied to sulfur composite (sulfur with filler particles). This approach is based on the concept of suspension, which consists of suspending fluid and suspended particles. Freshly mixed normal concrete, mortar, cement paste can be classified as suspension; concrete, mortar, and cement paste are a suspension of aggregates, fine sand, and cement respectively [18]. Sulfur products, made of sulfur and particle materials, also can be considered as a suspension of particles such as aggregates and filler. Thus, the rheological models for suspension materials can describe the sulfur composite and characterize the effect of different types of fillers.

2.3 Yield stress model for suspension materials

Yield stress is an important property to express the behavior of the particle-fluid suspension system. The study for the yield stress of suspension is less developed rather than the viscosity of suspension since there are difficulties in measuring the yield stress of suspension. The dilute suspension behaves like a Newtonian fluid with no yield stress, while the onset of yield stress is found at the suspension with high solid volume fraction, which behaves like non-Newtonian fluid [19]. In terms of interaction between particles, the behavior of the less concentrated suspension is hydrodynamic and after specific concentration is over transition point, the particles start to frictionally interact one another, influencing the rheology of suspension [20]. The specific solid volume fraction for the transition point, where the onset of yield stress occurs, is called percolation threshold. With the concept of percolation, the power law relationship between the yield stress and the solid volume fraction was numerically driven for the crystal-melt suspension, where the crystals forms crystal-network bridging the macroscopic samples, which results in the onset of yield stress (Eq. (2.3)) [21].

$$\tau_0 \propto (\varphi - \varphi_c)^{\beta} \tag{2.3}$$

In the relationship, τ_0 is yield stress, φ is the solid volume fraction, φ_c is percolation threshold, and β is a model constant. For the crystal-melt suspension, the power law exponent is from 2.5 to 3.5. This power law was also applied to the relationship between the yield stress and solid volume fraction in a subliquidus basalts [22]. Cement pastes with different amount of fly ash were fitted the power growth with the exponent of 4.5 [23].

2.4 Viscosity model for suspension materials

The behavior of suspension depends on the solid volume fraction or concentration of solid particles. As the solid volume fraction is higher, the viscosity of the suspension is higher. The relationship between the solid volume fraction and the viscosity of the suspension is well described by Krieger-Dougherty equation (Eq. (2.4)), which was derived by measuring the rheology of the suspension of mono-sized spherical latex particles [24].

$$\eta_r = \frac{\eta_s}{\eta_c} = (1 - \frac{\varphi}{\varphi_m})^{-[\eta]\varphi_m} \tag{2.4}$$

In the equation, η_r is the relative viscosity which is expressed as the ratio of the viscosity of the suspension, η_s and the viscosity of the continuous fluid, η_c. φ means the volume fraction occupied by solid particles and φ_m means the maximum packing volume fraction occupied by the solid particles

completely packed by external forces in specific volume. [η] is intrinsic viscosity for the solid particles. Since Krieger-Dougherty equation is derived from the mono-sized spherical particles, it fits well with the data for suspensions with the same shaped particles. In addition, the equation has been applied to the more complex suspensions such as submicron sphere, ground particles, and glass rods fibers. Intrinsic viscosity varies with the shape of the solid particles; [η] is 2.5 for a spherical particle, 3~5 for an equant particle, 4~10 for rod or fiber particles. The maximum packing volume fraction is also affected by not the size of the solid particles but the shape and size distribution of the solid particles. For example, the intrinsic viscosity of dispersed cement paste with superplasticizer is 5, where the cement particle is quite broad and has an elongate shape [25].

CHAPTER 3 – RHEOLOGY OF SULFUR COMPOSITE

3.1 Materials

3.1.1 Properties of modified sulfur and fillers

Dicyclopentadiene (DCPD)-modified sulfur was used as the binder of a sulfur composite, which was produced in the form of a yellow powder by Micro Powder, Inc. in Korea. Its specific gravity is 1.91. The blends of class F fly ash and Type I Portland cement were used for filler contents. Each specific gravity is 2.22 and 3.14, respectively. The oxide compositions for them were analyzed by XRF analysis and the results are shown in Table 3.1. Blends of fly ash and cement powder with various ratios produce a different particle size distribution of filler contents. The volumetric ratios of fly ash and cement are 1:0, 0.75:0.25, 0.5:0.5, 0.25:0.75, and 0:1, where each blend is labeled as F100, C25F75, C50F50, C75F25, and C100, respectively. The particle size distributions of each blend are analyzed by laser diffraction. As shown in Fig. 3.1, the particle size distributions for each filler particle are plotted, which shows the trend that the higher the cement content, the lower the median particle size. The median particle sizes of each blend (F100, C25F75, C50F50, C75F25, and C100) are listed in Table 3.2. It demonstrates the size of cement particle is smaller than that of fly ash.

Table 3.1 Oxide composition of Portland cement and fly ash obtained by XRF analysis

Label	CaO	SiO_2	Al_2O_3	Fe_2O_3	SO_3	MgO	K_2O	Na_2O
Cement	60.8%	21.1%	4.7%	3.2%	2.7%	2.1%	0.9%	0.3%
Fly ash	6.2%	52.3%	22.6%	9.1%	-	1.8%	1.8%	1.8%

Table 3.2 Volumetric ratio and median particle size of each blend of cement and fly ash

Label	Volumetric ratio (Cement:Fly ash)	Median particle size
C100	1:0	11.93 μm
C75F25	0.75:0.25	11.96 μm
C50F50	0.5:0.5	13.68 μm
C25F75	0.25:0.75	15.04 μm
F100	0:1	18.22 μm

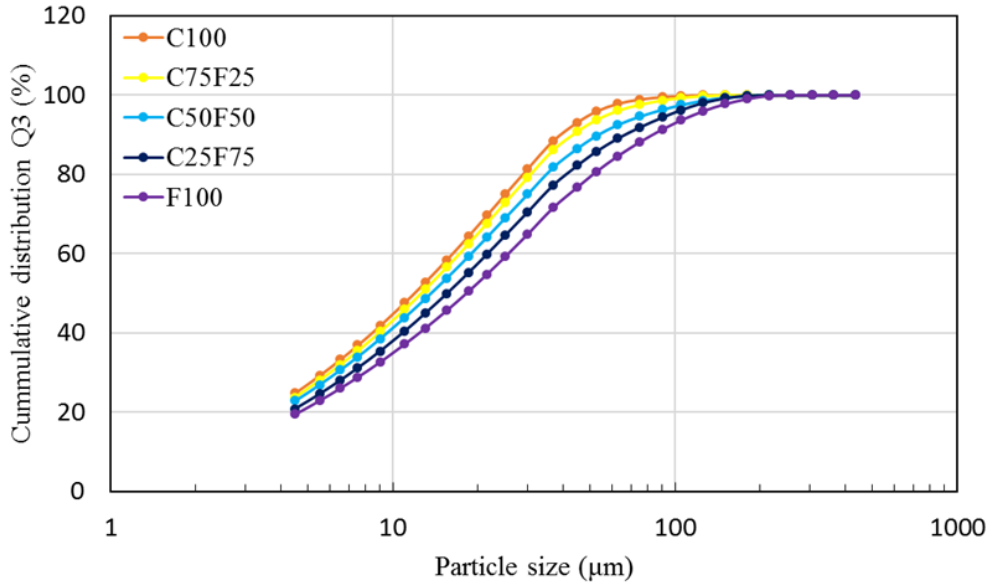

Figure 3.1 Cumulative particle distribution curves for each blend of cement and fly ash

3.1.2 Calculation of the number and the surface of filler particles in sulfur composite

As described in Fig. 3.2, assuming all the particles have a spherical shape, the total surface area and the number of particle in the composite was calculated with the measured density of each filler content. The result of particle size analysis produces how much weight of particles is portioned on each mesh size. Given that each particle between the adjacent meshes has a mono-sized diameter and each size of diameters equals to the average value of the adjacent mesh sizes (D_i), the volume ($V_{p,i}$) and the surface area ($A_{p,i}$) of one particle are expressed as below:

$$V_{p,i} = \frac{\pi}{6} D_i^3, \qquad A_{p,i} = \pi D_i^2 \tag{3.1), (3.2}$$

In the case of single cement or fly ash, the total volumes of particles between the adjacent meshes (V_i) are calculated by using the measured density (ρ_m) and the corresponding total weight of particles (m_i). The number of particles between the adjacent meshes (n_i) is obtained by Eq. (3.4).

$$V_i = \frac{m_i}{\rho_m} \tag{3.3}$$

$$n_i = \frac{V_i}{V_{p,i}} = \frac{6m_i}{\pi \rho_m D_i^3} \tag{3.4}$$

Then, the total number of particles (n) and the total surface area (A) of all the particles are obtained like below:

$$\mathrm{n} = \sum n_i, \qquad \mathrm{A} = \sum n_i A_{p,i} = \sum \frac{6m_i}{\rho_m D_i} \tag{3.5), (3.6}$$

Since cement and fly ash have a different range of size, the weight ratio of them (m_c:m_f) in each mesh size should be considered to calculate the total surface area of the blends of them. Fig. 3.3 shows the distribution density of C100 and F100, where the maximum sizes of fly ash and cement are 100 and 255 μm, respectively. If the volumetric ratio between the cement and fly ash is *a:b*, the total number of particles and the total surface area of blends of cement and fly ash is represented like below:

$$m_{i,c} = \frac{am_c}{am_c + bm_f}, \qquad m_{i,f} = \frac{bm_f}{am_c + bm_f} \tag{3.7), (3.8}$$

$$m_{i,c} \times \frac{1}{\rho_c} = V_{i,c}, \qquad m_{i,f} \times \frac{1}{\rho_f} = V_{i,f} \tag{3.9), (3.10}$$

$$n_{i,c} = \frac{V_{i,c}}{V_{p,i}}, \qquad n_{i,f} = \frac{V_{i,f}}{V_{p,i}} \tag{3.11), (3.12}$$

$$A_{i,c} = n_{i,c}A_{p,i}, \qquad A_{i,f} = n_{i,c}A_{p,i} \tag{3.13), (3.14}$$

$$\mathrm{n} = \sum n_{i,c} + n_{i,f}\,,\,,\,,\mathrm{A} = \sum n_{i,c}A_{p,i} + n_{i,f}A_{p,i} = \sum \frac{6m_{i,c}}{\rho_c D_i} + \frac{6m_{i,f}}{\rho_f D_i} \tag{3.15), (3.16}$$

Table 3.3 shows the total number of particles and surface area for each blend. Like the trend of the median particle size, the sulfur composites with higher cement content have a higher value of the total surface area and the number of the solid particle.

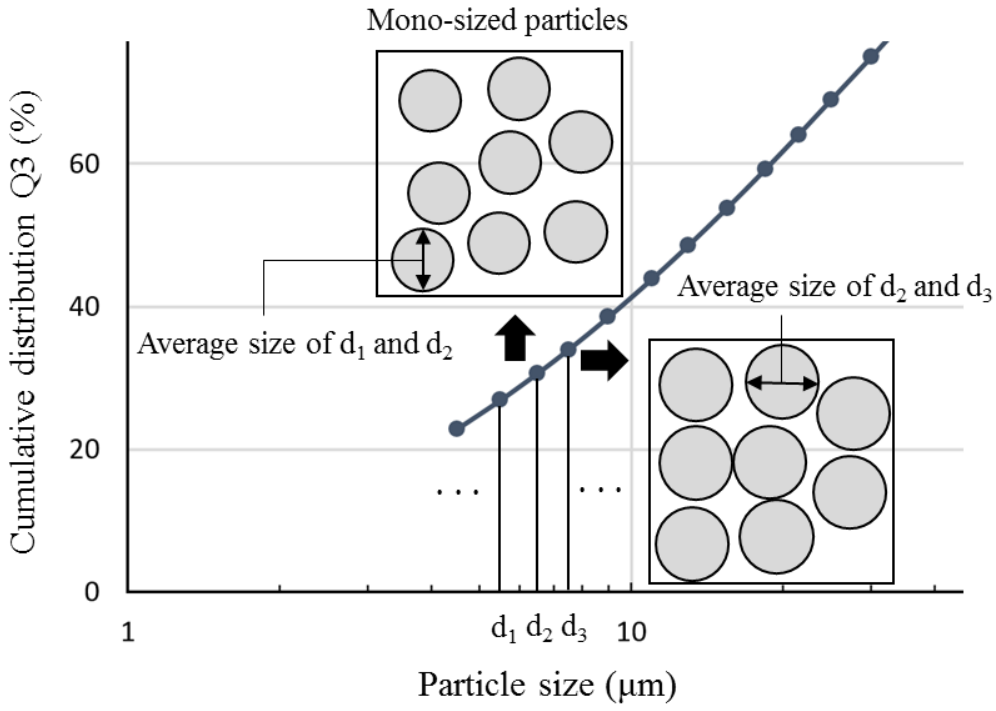

Figure 3.2 Particle distribution with assumption all the particles have a spherical shape and mono-sized diameter in each interval

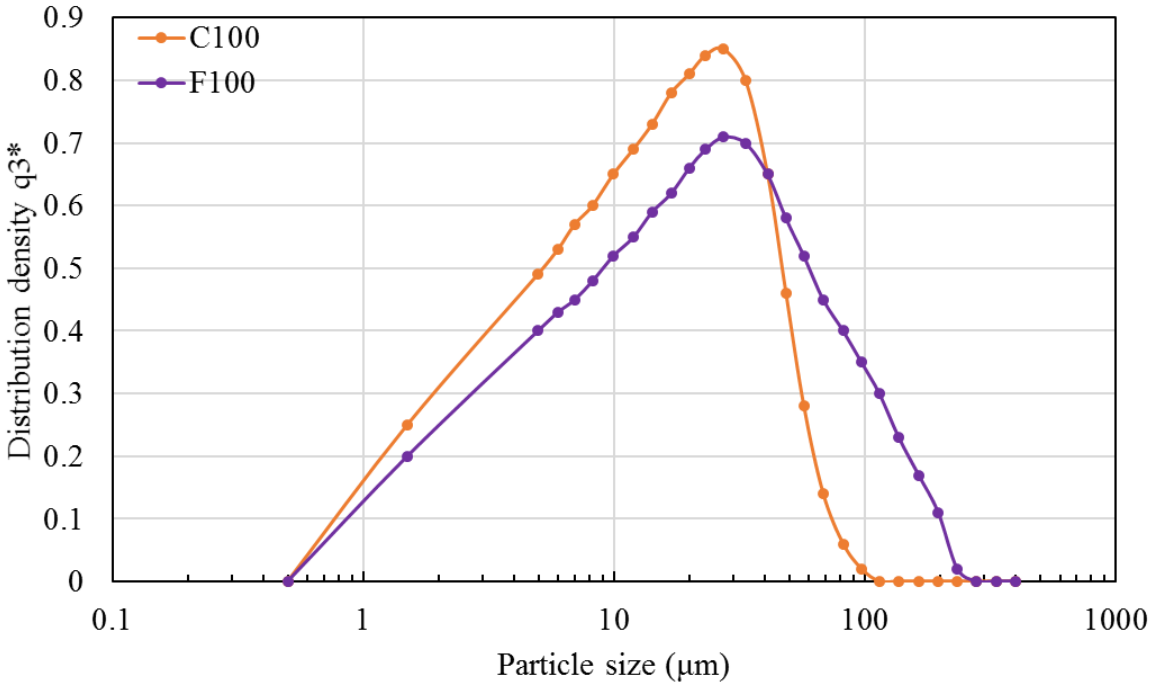

Figure 3.3 Particle size distribution of cement and fly ash

Table 3.3 Calculated surface area (based on 40 cm3 of filler and 200 cm3 of sulfur composite)

Label	Total number of particles	Particle number density (#/100μm^3)	Total surface area	Total surface area of particle / Volume of sulfur composite
C100	1.2791E+12	3.20	372448 cm^2	0.18622 cm^2/m^3
C75F25	1.2070E+12	3.02	354898 cm^2	0.17744 cm^2/m^3
C50F50	1.1519E+12	2.88	338862 cm^2	0.16943 cm^2/m^3
C25F75	1.0576E+12	2.64	316517 cm^2	0.15826 cm^2/m^3
F100	1.0019E+12	2.50	299499 cm^2	0.14975 cm^2/m^3

3.1.3 Maximum packing density of filler particles

In the particles just poured without any external forces except for gravity, there are voids between the particles. Applying external forces to the poured particles, the voids are occupied by other particles and the apparent volume of it seems to decrease, which process is called packing. When the particles are packed until there is no further increase in packing density, the maximum packing density(φ_m) is defined as the portion of the volume only occupied by the particles in the volume of particles including voids. In this study, the maximum packing density is measured by using a centrifuge (Fig. 3.4) [23]. For better packing results, the blends are centrifuged at 3000 rpm for 10 minutes after the cement and fly ash particles are well mixed. The volumes of centrifuged particles including voids were measured, and the volume of particles is calculated from the density of particles. Then the maximum packing density

is calculated by using the below equation:

$$\varphi_m = \frac{Volume\ \ of\ \ particles}{Volume\ \ of\ \ particles\ \ and\ \ voids} = \frac{V_p}{V_{packed,max}} = \frac{m/\rho_m}{V_{packed,max}} \quad (3.17)$$

Fig. 3.5 shows the volume reduction after maximum packing by the centrifuge. The higher the cement content, the lower the maximum packing density, which means the cement has more voids after packing. It demonstrates cement has lower maximum packing density due to its narrower size distribution of particles. Table 3.4 shows the calculated maximum packing densities of each blend of cement and fly ash.

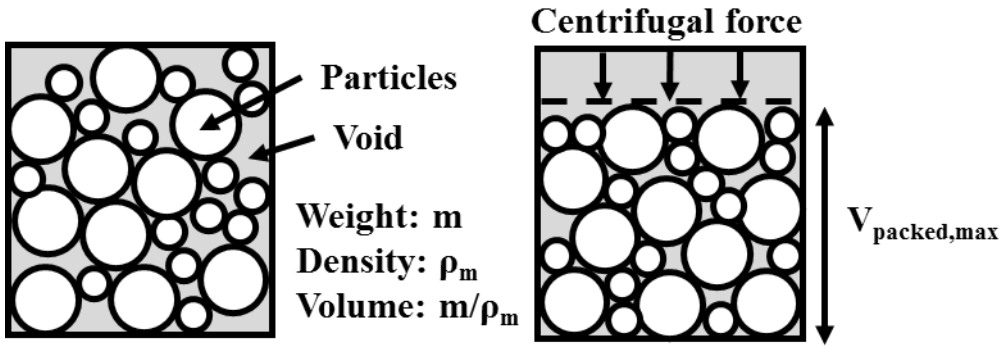

(a) **(b)**

Figure 3.4 (a) Particles in general state before packing, (b) Particles packed maximumly by centrifugal force

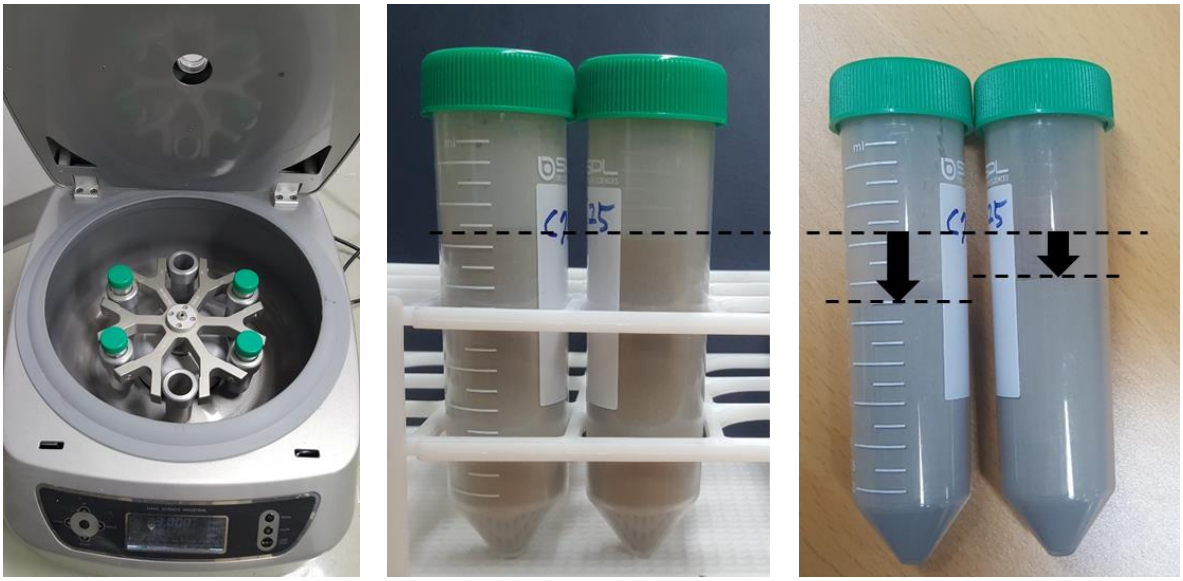

(a) **(b)** **(c)**

Figure 3.5 (a) Centrifuge, (b) C75F25 and C25F75 before packing, (c) C75F25 and C25F75 after maximum packing

Table 3.4 Calculated maximum packing densities

Label	Volume of particles and voids	Volume of particles	Maximum packing density
C100	26.25 cm^3	12.74 cm^3	0.49
	26.25 cm^3		0.49
C75F25	27.50 cm^3	13.75 cm^3	0.50
	27.38 cm^3		0.50
C50F50	28.13 cm^3	14.93 cm^3	0.53
	28.25 cm^3		0.53
C25F75	30.00 cm^3	16.33 cm^3	0.54
	29.90 cm^3		0.54
F100	30.78 cm^3	18.02 cm^3	0.59
	30.78 cm^3		0.59

3.2 Experimental procedure

3.2.1 Sample preparation

According to ACI committee 548 [26], the mix proportions for sulfur composites with a different filler content were designed at volumetric ratio. The filler volume is 20, 25, 30, 35% of the total volume of the sulfur composite. For each filler volume, 5 different blends from F100 to C100 were applied and the total mix designs are listed in Table 3.5 with their particle number density and total surface area of particles per volume of sulfur composite. Fig. 3.6 shows the protocol of mixing sulfur composite. Modified sulfur powder was placed into the heated pot. Stirring continuously, the constant heat was applied until modified sulfur gets fluidity. Then the filler was added into the molten sulfur and well mixed. After enough time to get the required temperature and homogeneity, the rheology of sulfur composite is measured.

Table 3.5 Mix design of sulfur composite

Filler	Label	Sulfur (g)	Cement (g)	Fly ash (g)	Particle number density	Total surface area particles / Volume of sulfur composite
20%	F100	305.6	0	88.8	2.50	0.150
	C25F75		31.4	66.6	2.64	0.158
	C50F50		62.8	44.4	2.88	0.169
	C75F25		94.2	22.2	3.02	0.177
	C100		125.6	0	3.20	0.186
25%	F100	286.5	0	111	3.13	0.187
	C25F75		39.3	83.3	3.31	0.198
	C50F50		78.5	55.5	3.60	0.212
	C75F25		117.8	27.8	3.77	0.222
	C100		157	0	4.00	0.233
30%	F100	267.4	0	133.2	3.76	0.225
	C25F75		47.1	99.9	3.97	0.237
	C50F50		94.2	66.6	4.32	0.254
	C75F25		141.3	33.3	4.53	0.266
	C100		188.4	0	4.80	0.279
35%	F100	248.3	0	155.4	4.38	0.262
	C25F75		55.0	116.6	4.63	0.277
	C50F50		109.9	77.7	5.04	0.297
	C75F25		164.9	38.9	5.28	0.311
	C100		219.8	0	5.60	0.326

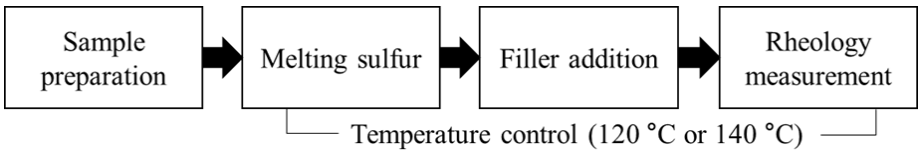

Figure 3.6 Mix and measurement process

3.2.2 Test protocol and temperature control

The rheometer records shear stress induced by according shear strain, which characterize the flow of sulfur composite quantitatively. The samples were measured for 160 seconds and Fig. 3.7 represents the shear rate history over time. During the first 30 seconds, relatively lower shear rate 1 1/s is applied for better contact between sample and the surface of plates. After 30 seconds, the shear rate is increased by 5 1/s every 20 seconds from 5 to 30 1/s. During the mixing sulfur composite, the heated pot controls the temperature of the sample. During the measurement of rheology, as shown in Fig. 3.8 (a), the furnace

controls the temperature of sample, which surrounds the parallel plates and keeps a constant temperature with hot air.

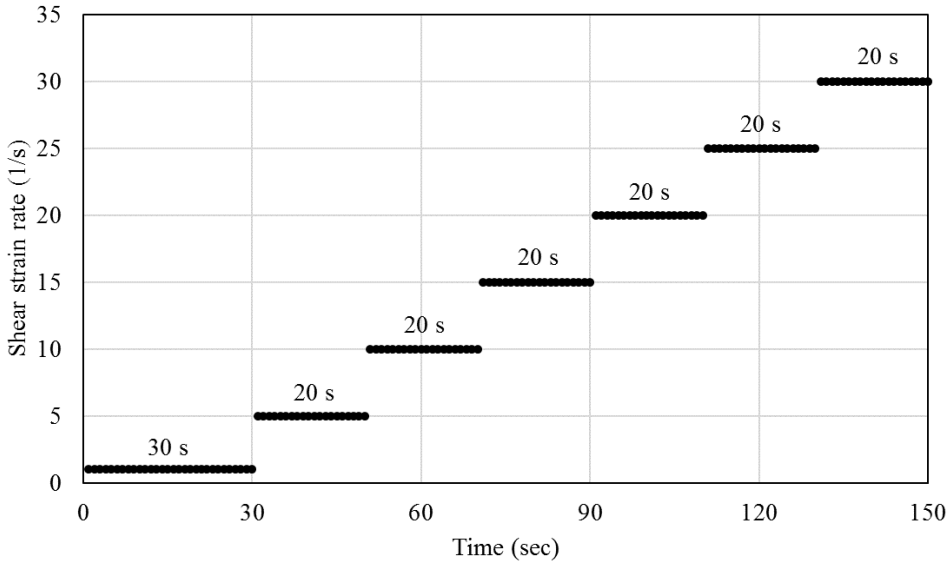

Figure 3.7 Shear strain rate history over times

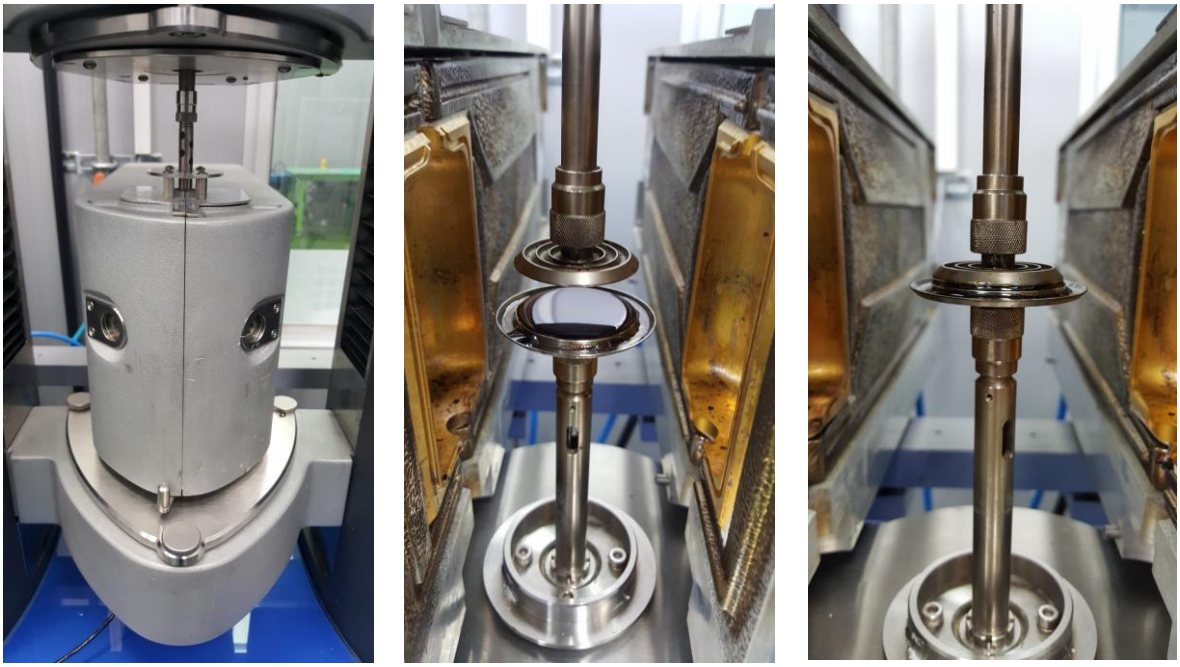

(a) **(b)** **(c)**

Figure 3.8 (a) Furnace controls the sample during the measurement of rheology, (b) Parallel plates in furnace after loading sulfur composite, (c) Parallel plates measuring the rheology of sulfur composite

3.2.3 Rheometer - parallel plates

The rheology of sulfur composites was measured by HAKKE MARS rheometer. Fig. 3.8 shows the overview of the rheometer. In detail, the samples are placed between the two plates with a diameter of 35 mm, called parallel plates, as described in Fig. 3.9. The parallel plate rotates with torque and angular velocity, which are instrument numbers recorded in the rheometer. For rheological analysis, the instrument numbers are needed to be converted to rheology numbers; shear stress and shear rate. The bottom plate is fixed and the upper plate rotates at given angular velocities. The gap size of them is set as 1 mm. Then, the placed sample has a shape of the cylinder like Fig. 3.9 (a). Since the bottom plate is fixed, the top surface of the cylinder sample, which is closest to the upper plate, has a maximum shear rate. From the definition of shear rate, the shear rate in the parallel plate can be expressed like below:

$$\dot{\gamma}(1/s) = \frac{V}{h} = \frac{\Omega r}{h} \tag{3.18}$$

, where h (m) is the distance from the bottom plate and V is a linear velocity (m/s). Linear velocity is expressed as a product of an angular velocity Ω (rad/s) and the distance from the center r (m). As shown in Fig. 3.9 (b), the circumference of the top surface of the cylinder has a maximum shear rate. Like the maximum shear rate, the maximum shear stress occurs at the circumference of the top surface. The maximum shear stress τ_{max} (Pa) caused by torque T (N·m) is express as Eq. (3.19).

$$\tau_{max} = \frac{T \times R}{J} = \frac{2T}{\pi R^3} \tag{3.19}$$

, where R is the radius of the top surface and J is a polar moment of area, which is expressed as $\pi/2 \cdot R^4$ in the cylinder. Based on the relationship between the maximum shear rates and shear stresses measured by parallel plates, the rheology of samples can be measured and analyzed.

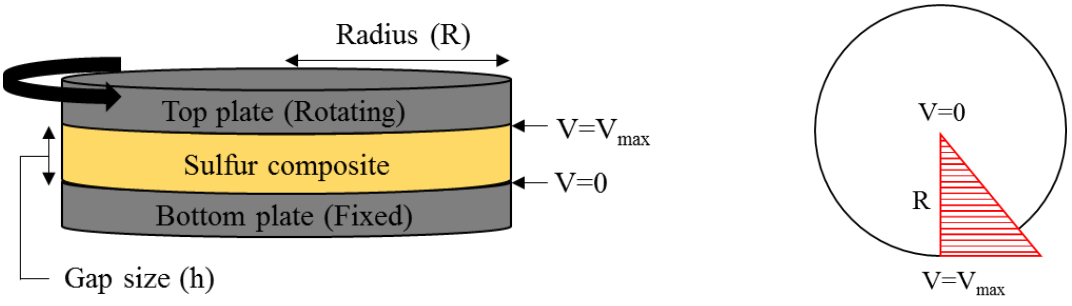

Figure 3.9 (a) Parallel plates with cylindrical sulfur composite, (b) Top surface of the sample

3.3 Flow curve

Flow curve describes the general flow behavior of materials, where the history of shear stress according to the protocol of shear strain rate is recorded. As mentioned in chapter 2, the representative analysis methods for linear and non-linear flow behavior are Bingham and Herschel-Bulkley models, both of which were applied to the result of measuring the sulfur composites.

3.3.1 Application of Bingham model

The yield stress and plastic viscosity of the sulfur composite were obtained by applying Bingham model. In the case of the sulfur composite with low filler contents, it shows linear behavior, where Bingham model shows a good fitting result like Fig. 3.10 (a). However, as the filler content is higher, the sulfur composite shows power growth, where the slope of tangent decreases as shear strain rate increases. The tangential slope is rapidly decreased at lower shear strain rate and gradually decreased at higher shear strain rate, as shown in Fig. 3.10 (b). Since the flow of higher filler contents is nonlinear, applying Bingham model for all rates describes the behavior of the sulfur composite inaccurately. To increase the accuracy of the fitting, Bingham model can be selectively applied to the certain shear strain rates having a small rate of change of slope. In Fig. 3.10 (d), the shear strain rate of 1~10 1/s is excluded due to the rate of change and the shear strain rate of 20~30 1/s is also excluded since the shear strain rate of 10~20 1/s shows better results like Fig. 4.1~4.5.

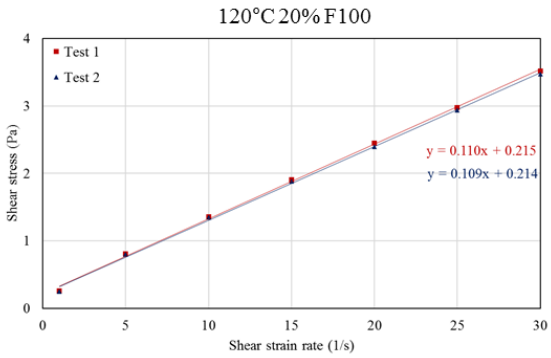

(a)

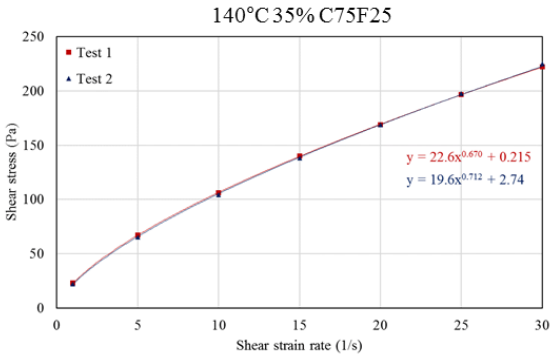

(b)

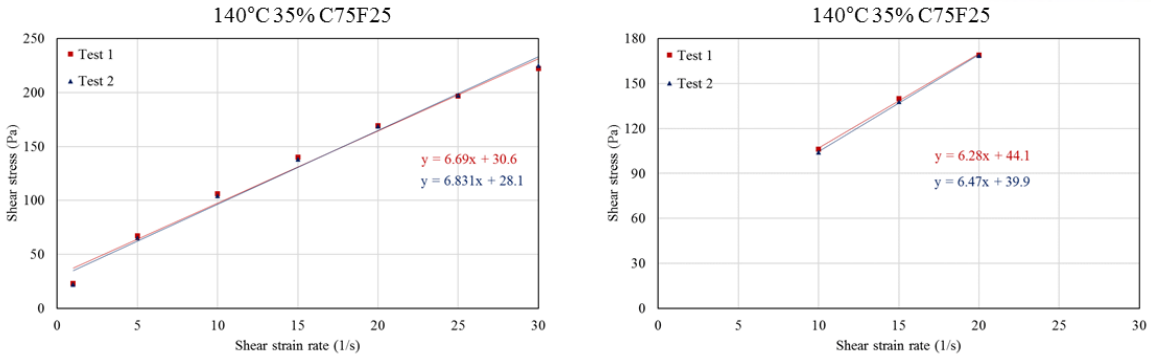

(c) **(d)**

Figure 3.10 (a) Bingham model applied for 120°C 20% F100, (b) Herschel-Bulkley model applied for 140°C 35% C75F25, (c) Bingham model applied for 140°C 35% C75F25, (d) Bingham model applied for 140°C 35% C75F25 at the shear strain rate of 10, 15, 20 1/s

3.3.2 Application of Herschel-Bulkley model

Herschel-Bulkley model well describes the behavior of the sulfur composite with higher filler contents. As mentioned in Chapter 2, Herschel-Bulkley model is characterized by three model constants a, b, and c, which mean viscosity at the shear strain rate of 1 1/s, exponent, and yield stress, respectively. Fig. 3.11 describes the trend of the three model constants according to the surface area of filler particles, applying Herschel-Bulkley model to the sulfur composites measured in 120 °C. Compared to the trend of viscoisty obtained by Bingham model in Fig. 4.3, the viscosity shows a similar continuous growth except for C75F25 and C100 samples in each filler content. It demonstrates the effect of the surface area of particles to the viscosity is different depending on the range of shear strain rate. The exponents show the upside down reversed trend of the viscosity at 1 1/s. The yield stress of each group having the same total filler content has a discontinuous power growth, which trend is similar to the results analyzed by Bingham model in Fig 4.1.

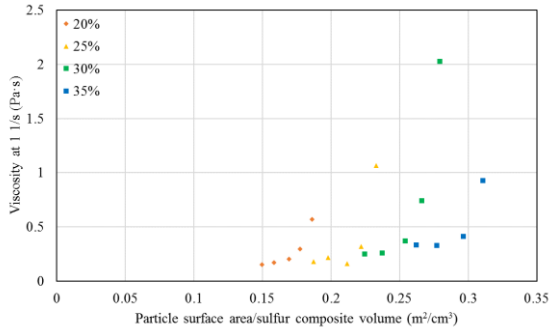

(a)

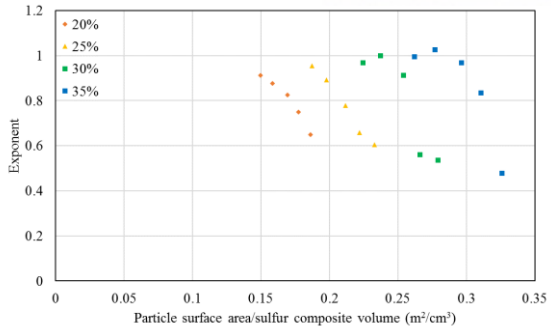

(b)

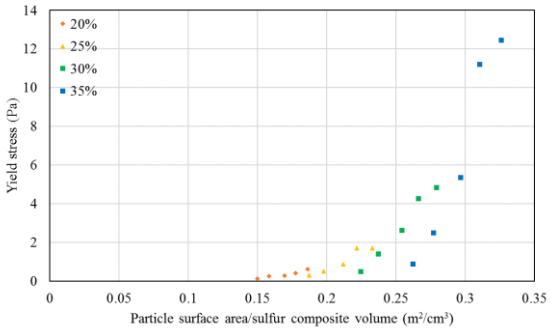

(c)

Figure 3.11 (a) Viscosity at shear strain rate of 1 1/s, (b) exponents, and (c) yield stress depending on the particle surface area

CHAPTER 4 – RESULT AND DISSCUSION

4.1 Rheological properties: yield stress and viscosity

4.1.1 Yield stress depending on the surface area of particles in sulfur composite

Yield stress and plastic viscosity were measured by applying Bingham model at the shear strain rate of 10~20 1/s. As shown in Fig. 4.1, in the group of sulfur composites with same volume fractions of filler, the sulfur composite with higher cement content produces higher yield stress. However, the general trend of yield stress and particle surface area shows a discontinuous growth when the sulfur composite has a different volume fraction of filler. For example, 30% C100 (0.279 m^2/cm^3) and 35% C25F75 (0.277 m^2/cm^3) have similar particle surface area but the yield stress of 35% C2575 is remarkably low. It demonstrates the other characteristics of filler, rather than total surface area, are more influential in producing the yield stress of sulfur composite. As shown in Fig. 4.2, the trends of yield stress and particle surface area of each filler type represent a continuous power growth of yield stress. If the same type of filler is used, the yield stress of sulfur composites is proportional to the particle surface area and the volume fraction of the filler, which is consistent with the description of the yield stress model for suspensions.

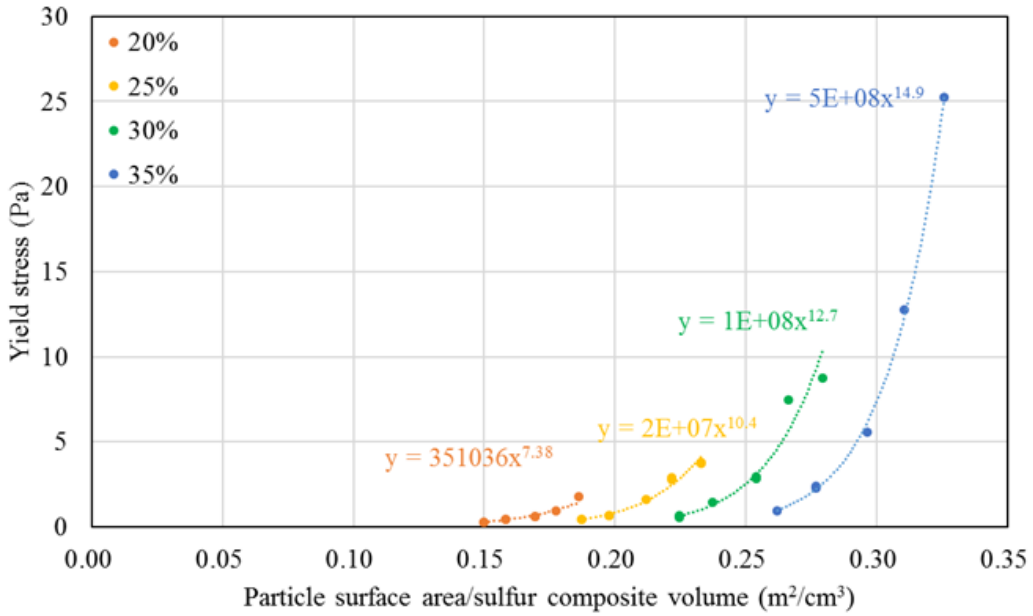

(a) 120 °C

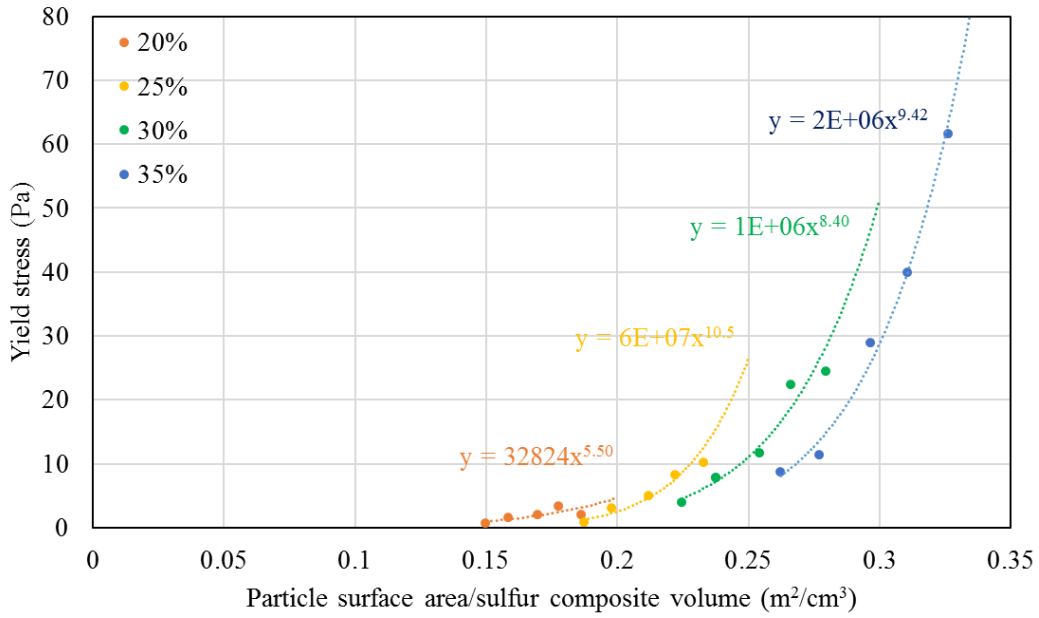

(b) 140 °C

Figure 4.1 The relationship between the yield stress of the sulfur composite and particle surface area of the filler based on the total amount of filler contents (a) at 120 °C (b) at 140 °C.

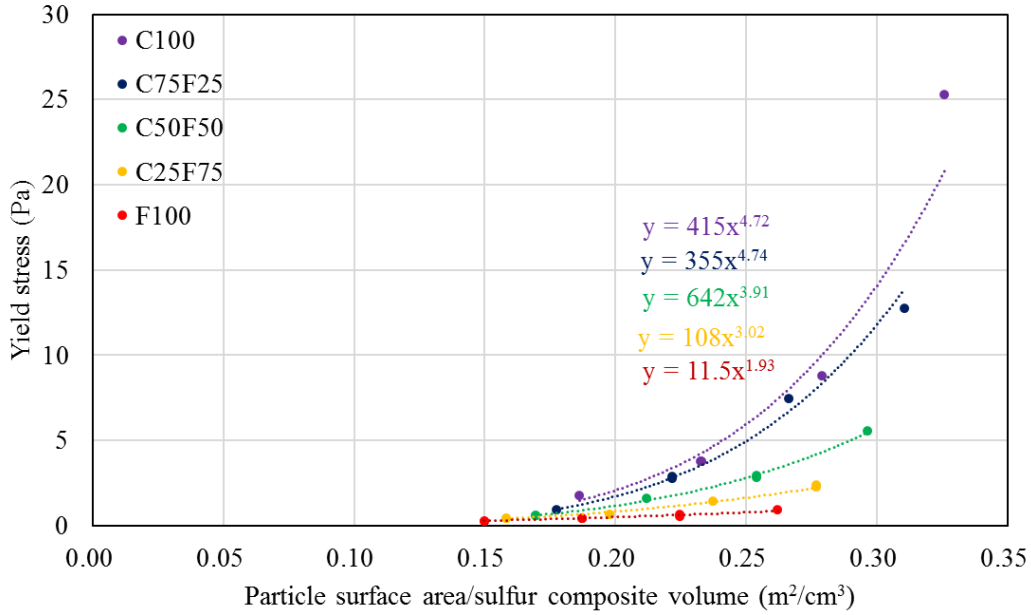

(a) 120 °C

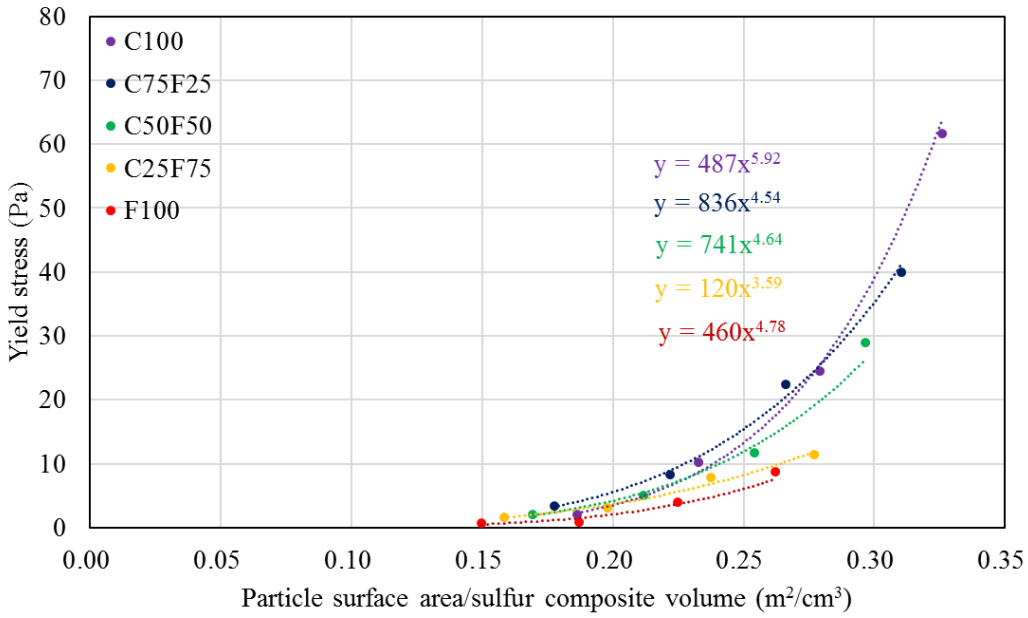

(b) 140 °C

Figure 4.2 The relationship between the yield stress of the sulfur composite and particle surface of the filler based on the mixing ratio of cement and fly ash

4.1.2 Viscosity depending on the surface area of particles in sulfur composite

Fig. 4.3 shows the trend of viscosity according to the surface area of the filler particles in the sulfur composite. Compared to the trend in yield stress, viscosity clearly shows power growth with increasing surface area of filler regardless of mixing ratio between cement and fly ash. For example, 25% C100 (0.233 m^2/cm^3) and 30% C25F75 (0.237 m^2/cm^3) have a different filler ratio of cement and fly ash but the viscosity of them fits well to the overall trend of viscosity according to the particle surface area in the sulfur composite. It demonstrates the surface area of filler particles strongly affect the viscosity of sulfur composite.

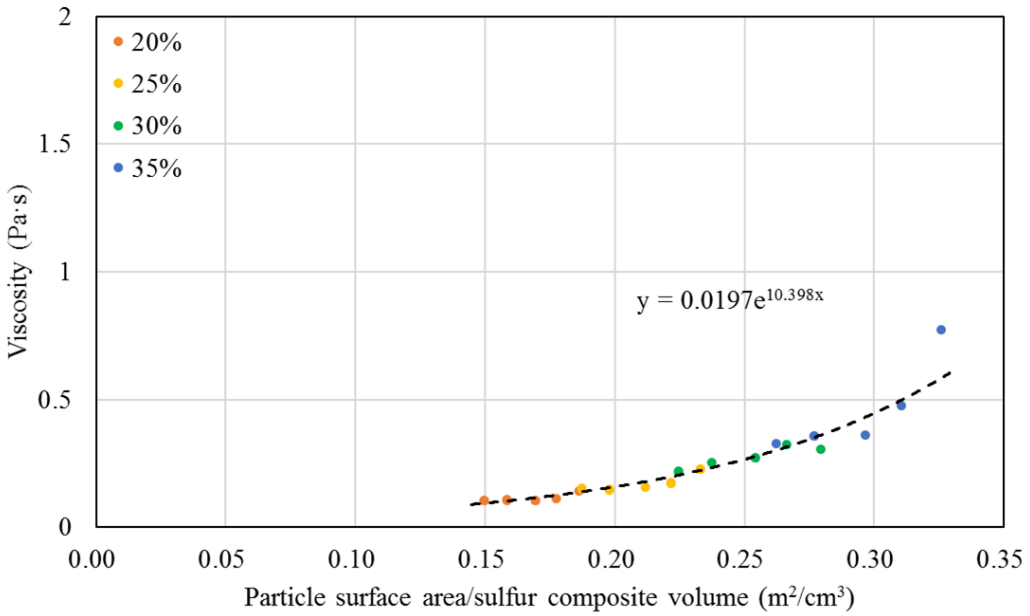

(a) 120 °C

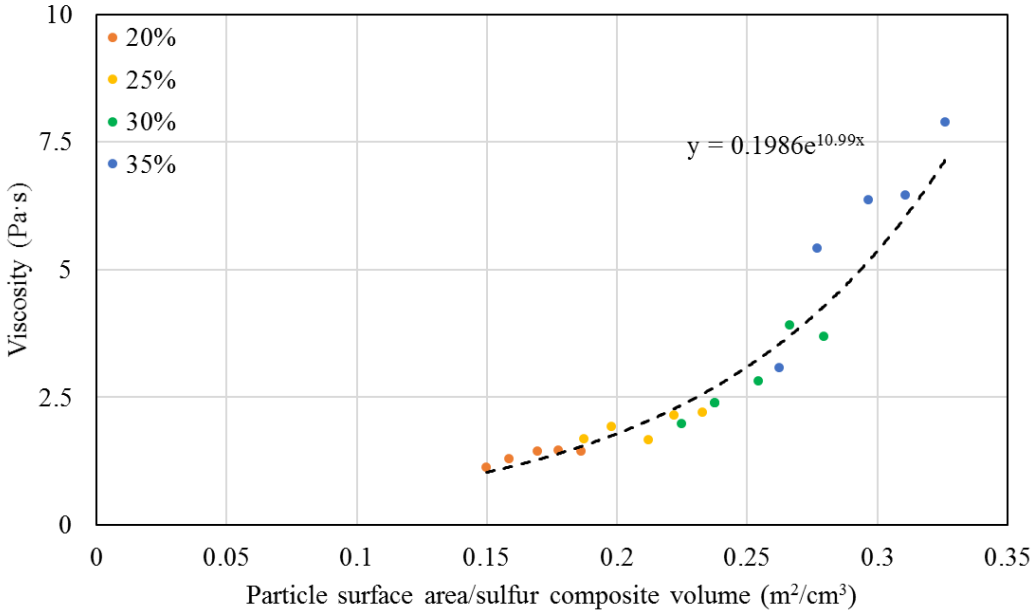

(b) 140 °C

Figure 4.3 The relationship between the viscosity of the sulfur composite and particle surface area or the filler

4.2 Model fitting

4.2.1 Application of yield stress model

The factors to be considered in the yield stress model are how the model constants and the percolation thresholds are determined according to the characteristics of the filler. Fig. 4.4 shows the growth in yield stress depending on the volume fraction of the filler. For each filler type, the yield stress shows the power growth with the increasing volume fraction of the filler. Taking log on both sides of the model represents the linear behavior of yield stress in log scale, where the slope and y-intercept increase with the higher portion of cement. It implies the properties of the particles affect the coefficient and exponent in the yield stress model. From Fig. 4.4 (a)~(d), the yield stress is proportional to the volume fraction of the filler from 20% to 35%, which means the percolation threshold is less than 0.2 and it is negligible when the filler content is above 20%.

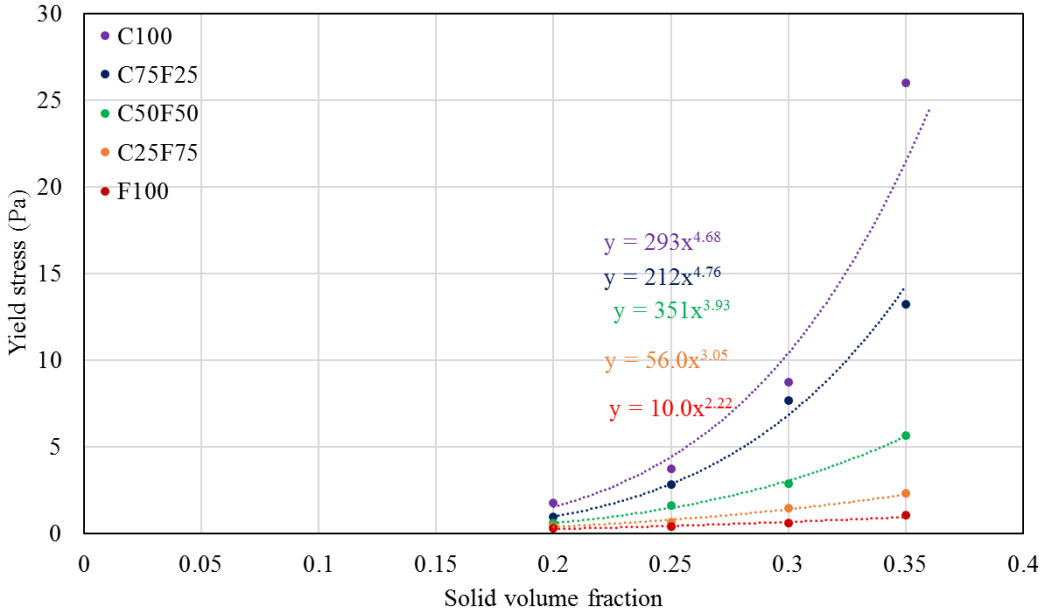

(a) **120 °C**

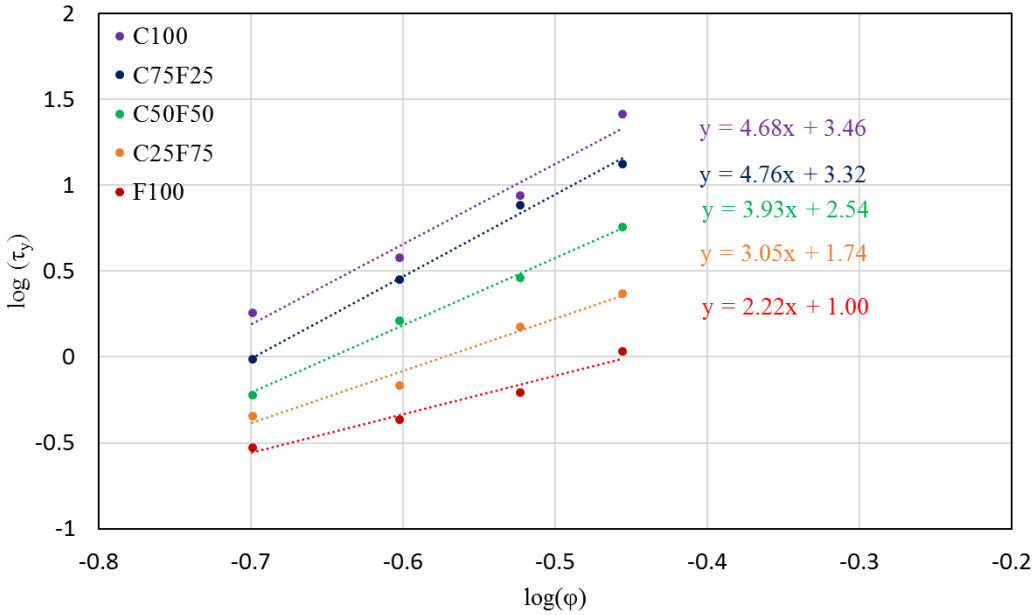

(b) **120 °C (log scale)**

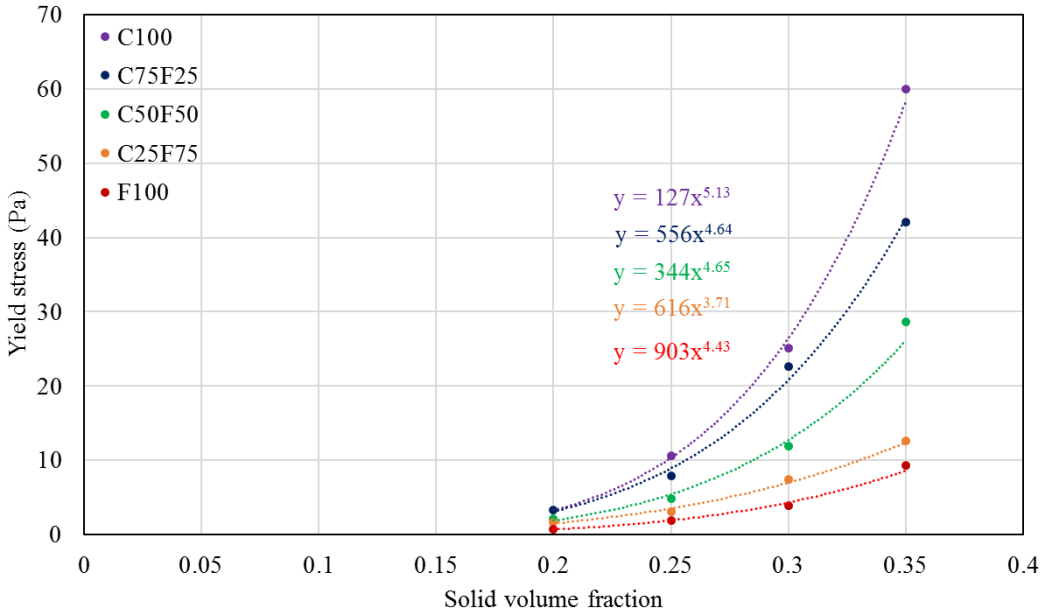

(c) **140 °C**

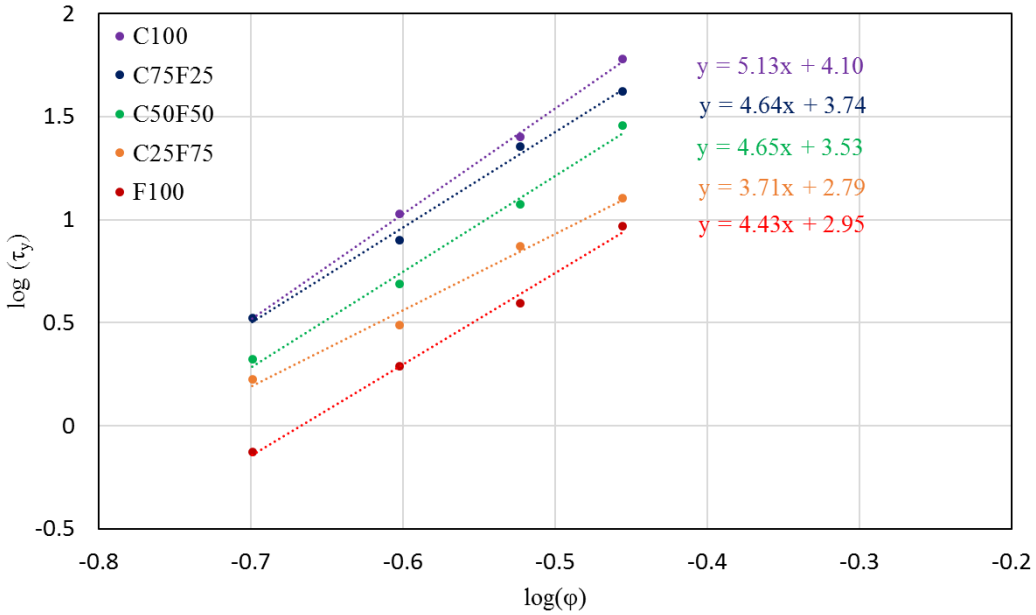

(d) **140 °C (log scale)**

Figure 4.4 The relationship between the yield stress of sulfur composite and the solid volume fraction of the filler

4.2.2 Application of viscosity model

In the viscosity model, relative viscosity is measured by rheometer, volume fraction was set from the mix design, and the maximum packing density is measured by the centrifuge test. The only unknown variable is intrinsic viscosity. Intrinsic viscosity indicates how much the suspended particles influence the rheological properties of the suspension, which varies with the shape and size distribution of particles. When the blends of two particles are used, the intrinsic viscosity of the blends can be calculated by considering the volumetric ratio and intrinsic viscosity of each particle like Eq. (4.1) [23].

$$[\eta] = \frac{V_{cem}}{V_{cem} + V_{FA}}[\eta]_{cem} + \frac{V_{FA}}{V_{cem} + V_{FA}}[\eta]_{FA} \quad (4.1)$$

where, $[\eta]_{cem}$, $[\eta]_{FA}$, and $[\eta]$ are the intrinsic viscosity of cement, fly ash, and the blends of them and V_{cem} and V_{FA} is the volume fraction of cement and fly ash in the blends of them, respectively. Table 4.1 shows the intrinsic viscosity of F100 and C100 obtained from fitting the results to Krieger-Dougherty Equation (Eq. (2.4)). Regardless of the volume fraction of filler, the obtained intrinsic viscosities in the same label have a similar value and the average value of them is used for the representative value, where the relative viscosity is measured twice, which are η_{r1} and η_{r2}, for each volume fraction. Based on the intrinsic viscosity of F100 and C100, the intrinsic viscosity of each blend of cement and fly ash is calculated by Eq. (2.4) and the results are shown in Table 4.2.

Fig. 4.5 compares the relative viscosity from Krieger-Dougherty equation and the calculated intrinsic viscosity and the relative viscosity measured by parallel plates. In the case of 120 °C, the measured relative viscosity of 30% C100 is 20.23% lower, those of 35F C25F75, C50F50, and C75F25 are 12.42%, 29.69%, and 25.13% lower, respectively. For other samples with the relative viscosity of 8 or less, the measured relative viscosities are similar with the calculated relative viscosities. In the case of 140 °C, the measured relative viscosities of 30% C75F75 and 35% C25F75, C50F50, C75F25, and C100 are 20.38%, 37.03%, 37.49%, 19.54%, 19.93% higher, respectively. For other samples with the relative viscosity of 5 or less, the measured relative viscosities and the calculated relative viscosities are well matched each other.

Table 4.1. Intrinsic viscosity of C100 and F100 calculated by Krieger-Dougherty equation

Temp.	Label	φ	η_{s1}	η_{s2}	φ_m	η_c	η_{r1}	η_{r2}	$[\eta]_1$	$[\eta]_2$	$[\eta]$
120 °C	F100	0.2	0.11	0.11	0.59	0.043	2.53	2.45	3.79	3.66	3.80
		0.25	0.15	0.15			3.47	3.52	3.81	3.86	
		0.30	0.26	0.25			5.15	5.02	3.90	3.84	
		0.35	0.36	0.36			7.36	7.58	3.74	3.80	
	C100	0.20	0.14	0.14	0.49	0.043	3.33	3.27	4.66	4.60	4.54
		0.25	0.23	0.23			5.28	5.27	4.74	4.73	
		0.30	0.30	0.29			7.10	6.76	4.19	4.09	
		0.35	0.76	0.77			17.56	18.00	4.62	4.66	
140 °C	F100	0.2	1.11	1.13	0.59	0.6	1.86	1.89	2.52	2.59	2.85
		0.25	1.43	1.70			2.38	2.83	2.66	3.19	
		0.30	1.99	2.13			3.32	3.55	2.86	3.01	
		0.35	2.82	3.07			4.70	5.12	2.90	3.06	
	C100	0.20	1.44	1.57	0.49	0.6	2.41	2.61	3.41	3.72	3.80
		0.25	2.14	2.21			3.56	3.68	3.62	3.71	
		0.30	3.48	3.69			5.81	6.15	3.76	3.89	
		0.35	7.94	7.90			13.24	13.16	4.17	4.16	

Table 4.2. Calculated intrinsic viscosity of each blend of cement and fly ash

Label	$[\eta]$ for 120 °C	$[\eta]$ for 140 °C
F100	3.799	2.850
C25F75	3.983	3.088
C50F50	4.168	3.327
C75F25	4.353	3.565
C100	4.537	3.804

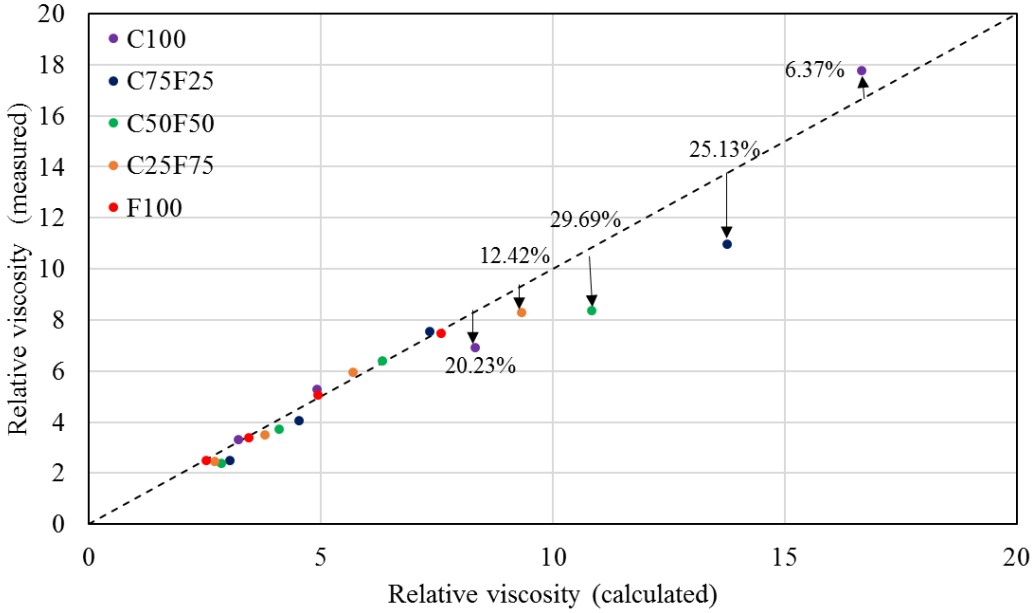

(a) 120 °C

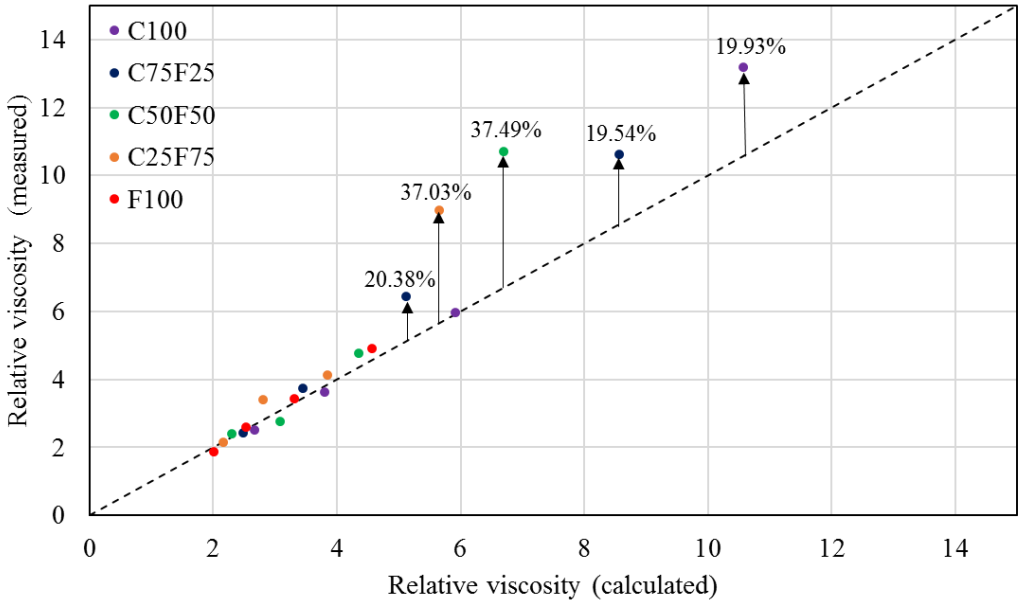

(b) 140 °C

Figure 4.5 The comparison of the relative viscosity predicted by Krieger-Dougherty equation with the relative viscosity measured by parallel plates

4.3 Effects of excessive use of filler to the rheology of sulfur composite

4.3.1 Sedimentation of filler particles in sulfur composite

Fig. 4.5 (a) represents the samples with the relative viscosity above 8 have a less relative viscosity than the calculated one. Since sulfur at 120 °C has quite lower yield stress and viscosity than at 140 °C, it has a lower capability to suspend the filler particles, which results in partial sedimentation of filler particles [27]. Sedimentation refers to the separation of particles and fluid, where the particles are relatively concentrated at the bottom place due to gravity. Since parallel plates measure the shear stress at the top surface of the sample, the sedimentation makes the upper part of sulfur composite more dilute and reduces the effect of particles on the rheological properties.

4.3.2 Frictional interaction and hydrodynamic interaction between particles in suspension

In suspension system, the mechanism of interaction between the suspended particles changes depending on the shear strain rate and the volume fraction of suspended particles [28]. For example, the yield stress of the freshly-mixed normal concrete with a different volume fraction of aggregates has a different trend depending on the range of the volume fraction. As the volume fraction of aggregates increases, the frictional effect of particles becomes dominant rather than hydrodynamic effect [20]. Frictional contact between the particles induces more increase in not only the yield stress but also viscosity. As shown in Fig. 4.5 (b), the samples with the relative viscosities above 5, most of which have 35% filler content, have a higher relative viscosity than the calculated one. It is because Krieger-Dougherty equation is derived without considering the frictional effect of particles and has been verified for soft suspension, which has a lower volume fraction of particles. The sedimentation of filler and frictional effect, which occurred mostly above 35% filler content, contribute to the difficulty of performance evaluation of sulfur composite; there are 10~30% overestimate and underestimate of viscosity.

CHAPTER 5 – CONCLUSIONS

5.1 Conclusions

In this study, the effect of filler on the rheology of sulfur composites was investigated as a basic data for the quantitative evaluation of workability of sulfur concrete. The yield stress and plastic viscosity were investigated by varying the characteristics of filler in the sulfur composite such as the volume fraction, particle size distribution, and total surface area of the filler. In the flow curve obtained from the rheometer: parallel plates, the sulfur composite with low volume fraction of filler showed a linear behavior and the sulfur composite with high volume fraction of filler had a nonlinear behavior. Analysis of the flow curve through the Bingham model and Herschel Bulkley model represented the application of the Bingham model at a shear strain rate of 10 to 20 1/s best describes the effect of filler characteristics on rheological properties. The yield stress tends to increase with the surface area of the filler when the total amount of filler is constant, and the yield stress increases discontinuously with respect to the surface are of the filler in overall. In terms of volume fraction, the yield stress of sulfur composite with the same type of filler shows continuous power growth. Applying the conventional yield stress model represents model constants, the coefficient and exponent, were depending on the type of filler. It demonstrates the yield stress of sulfur composite is described mainly by volume fraction and the degree of increase in yield stress is depending on the type of the filler. The viscosity of sulfur composite shows continuous power growth with the increasing the surface of filler particles regardless of the type of filler. It demonstrates the viscosity of sulfur composite is mainly affected by the surface area of the filler. In Krieger-Dougherty model, the intrinsic viscosity is characterized by the type of filler. The intrinsic viscosity of blends of two type of filler can be predicted by considering the volumetric ratio and the intrinsic viscosity of each type of filler. The predicted intrinsic viscosity and Krieger-Dougherty model produced the calculated (predicted) relative viscosities of the sulfur composite. Generally, the sulfur composites with the volume fraction of the filler of 30% or less at both 120 and 140 °C show good agreement with the predicted relative viscosity and the measured relative viscosity. When the filler is added excessively like the sulfur composites with the volume fraction of 35%, the sedimentation or frictional interaction between the filler particles occurs depending on the rheological properties of the suspending sulfur. The models for the rheological properties of the suspension were well applied to the sulfur composite within the range of proper addition of filler. Thus, sulfur composites are considered as suspensions and various suspension theories can be applied to the sulfur composite.

REFERENCES

1. Mohamed, A. M. O., & El-Gamal, M. (2010). *Sulfur concrete for the construction industry: a sustainable development approach*. J. Ross Publishing.
2. Mohamed, A. M. O., & El Gamal, M. (2007). Sulfur based hazardous waste solidification. *Environmental geology*, *53*(1), 159-175.
3. Bacon, R.F. & Davis, H.S. (1921). Recent advances in the American sulfur industry. Chem Metallurgical Eng 24(2), 65–72
4. Gregor, R., & Hackl, A. (1978). A new approach to sulfur concrete.
5. Voronkov, M. G., & Lapina, T. V. (1966). The reaction of sulfur with organic compounds. Chemistry of Heterocyclic Compounds, 1(3), 224-228.
6. Blight, L., Currell, B. R., Nash, B. J., Scott, R. A. M., & Stillo, C. (1978). Preparation and properties of modified sulfur systems.
7. Bahrami Adeh, N., Mohtadi Haghighi, M., & Mohammad Hosseini, N. (2008). Preparation of Sulfur Mortar from Modified Sulfur. Iranian Journal of Chemistry and Chemical Engineering (IJCCE), 27(1), 123-127.
8. ASTM C39 Standard Test Method for Compressive Strength of Cylindrical Concrete Specimens
9. ASTM C78 Standard Test Method for Flexural Strength of Concrete (Using Simple Beam with Third-Point Loading)
10. ASTM C496 Standard Test Method for Splitting Tensile Strength of Cylindrical Concrete Specimens
11. Roussel, N., & Coussot, P. (2005). "Fifty-cent rheometer" for yield stress measurements: from slump to spreading flow. Journal of rheology, 49(3), 705-718.
12. Martinie, L., Rossi, P., & Roussel, N. (2010). Rheology of fiber reinforced cementitious materials: classification and prediction. Cement and Concrete Research, 40(2), 226-234.
13. ASTM C143 Standard Test Method for Slump of Hydraulic-Cement Concrete
14. Tregger, N., Ferrara, L., & Shah, S. P. (2008). Identifying viscosity of cement paste from mini-slump-flow test. ACI Materials Journal, 105(6), 558.
15. Mahmoodzadeh, F., & Chidiac, S. E. (2013). Rheological models for predicting plastic viscosity and yield stress of fresh concrete. Cement and Concrete Research, 49, 1-9.
16. McBee, W. C., & Weber, H. H. (1990, August). Sulfur polymer cement concrete. In Proceedings of the Twelfth Annual Department of Energy Low-level Waste Management Conference CONF-9008119 National Low-Level Waste Management Program, Idaho Natl. Engineering Lab., Idaho Falls, Idaho.
17. Makenya, A. R. (1997). Composition for durability of a chempruf-modified sulfur concrete (Doctoral dissertation, Institutionen för arkitektur).
18. Toutou, Z., & Roussel, N. (2006). Multi scale experimental study of concrete rheology: from water scale to gravel scale. Materials and Structures, 39(2), 189-199.
19. Jeffrey, D. J., & Acrivos, A. (1976). The rheological properties of suspensions of rigid particles. AIChE Journal, 22(3), 417-432.
20. Yammine, J., Chaouche, M., Guerinet, M., Moranville, M., & Roussel, N. (2008). From ordinary rhelogy concrete to self compacting concrete: A transition between frictional and hydrodynamic interactions. Cement and Concrete Research, 38(7), 890-896.
21. Walsh, S. D., & Saar, M. O. (2008). Numerical models of stiffness and yield stress growth in crystal-melt suspensions. Earth and Planetary Science Letters, 267(1-2), 32-44.
22. Hoover, S. R., Cashman, K. V., & Manga, M. (2001). The yield strength of subliquidus basalts—experimental results. Journal of Volcanology and Geothermal Research, 107(1-3), 1-18.
23. Bentz, D. P., Ferraris, C. F., Galler, M. A., Hansen, A. S., & Guynn, J. M. (2012). Influence of particle size distributions on yield stress and viscosity of cement–fly ash pastes. Cement and Concrete Research, 42(2), 404-409.
24. Krieger, I. M., & Dougherty, T. J. (1959). A mechanism for non-Newtonian flow in suspensions of rigid spheres. Transactions of the Society of Rheology, 3(1), 137-152.
25. Struble, L., & Sun, G. K. (1995). Viscosity of Portland cement paste as a function of concentration. Advanced Cement Based Materials, 2(2), 62-69.

26. ACI committee 548.1R-97 Guide for the Use of Polymers in Concrete
27. Chan, A. K., & Chaffey, C. E. (1992). Increased sedimentation rate and viscosity in suspensions of humidified glass beads. Chemical engineering science, 47(17-18), 4471-4473.
28. Coussot, P., & Ancey, C. (1999). Rheophysical classification of concentrated suspensions and granular pastes. Physical Review E, 59(4), 4445.

ACKNOWLEDGMENTS

I would like to thank all members in UEE. Especially, I would like to thank Professor Myoungsu Shin for his generous support for my research while writing my thesis. Also, I would like to thank Seongwoo Gwon for giving me a lot of information about sulfur.

APPENDIX

The relationship between shear stress and shear strain rate of sulfur composite at 120 °C

20%									
F100		C25F75		C50F50		C75F25		C100	
τ (Pa)	γ̇ (1/s)	τ (Pa)	γ̇ (1/s)	τ (Pa)	γ̇ (1/s)	τ (Pa)	γ̇ (1/s)	τ (Pa)	γ̇ (1/s)
0.251	1	0.394	1	0.479	1	0.690	1	1.178	1
0.798	5	0.946	5	1.088	5	1.429	5	2.307	5
1.348	10	1.499	10	1.650	10	2.056	10	3.173	10
1.887	15	2.035	15	2.167	15	2.649	15	3.897	15
2.400	20	2.561	20	2.685	20	3.183	20	4.580	20
2.936	25	3.065	25	3.175	25	3.711	25	5.229	25
3.474	30	3.555	30	3.666	30	4.195	30	5.834	30
25%									
F100		C25F75		C50F50		C75F25		C100	
τ (Pa)	γ̇ (1/s)	τ (Pa)	γ̇ (1/s)	τ (Pa)	γ̇ (1/s)	τ (Pa)	γ̇ (1/s)	τ (Pa)	γ̇ (1/s)
0.476	1	0.686	1	1.333	1	2.371	1	2.738	1
1.178	5	1.365	5	2.229	5	3.566	5	4.696	5
1.927	10	2.122	10	3.040	10	4.518	10	5.990	10
2.684	15	2.825	15	3.911	15	5.395	15	7.172	15
3.418	20	3.557	20	4.715	20	6.245	20	8.255	20
4.163	25	4.266	25	5.512	25	7.117	25	9.154	25
4.936	30	4.947	30	6.292	30	7.899	30	10.186	30
30%									
F100		C25F75		C50F50		C75F25		C100	
τ (Pa)	γ̇ (1/s)	τ (Pa)	γ̇ (1/s)	τ (Pa)	γ̇ (1/s)	τ (Pa)	γ̇ (1/s)	τ (Pa)	γ̇ (1/s)
0.733	1	1.619	1	2.839	1	6.198	1	6.807	1
1.714	5	2.737	5	4.227	5	8.812	5	9.735	5
2.821	10	3.996	10	5.594	10	10.664	10	11.790	10
3.882	15	5.237	15	6.930	15	12.302	15	13.398	15
4.978	20	6.518	20	8.326	20	13.891	20	14.841	20
6.081	25	7.823	25	9.678	25	15.325	25	16.250	25
7.186	30	9.160	30	11.095	30	16.809	30	17.410	30
35%									
F100		C25F75		C50F50		C75F25		C100	
τ (Pa)	γ̇ (1/s)	τ (Pa)	γ̇ (1/s)	τ (Pa)	γ̇ (1/s)	τ (Pa)	γ̇ (1/s)	τ (Pa)	γ̇ (1/s)
1.186	1	2.745	1	5.693	1	11.943	1	17.347	1
2.602	5	4.171	5	7.425	5	15.147	5	27.427	5
4.193	10	5.894	10	9.182	10	17.525	10	32.913	10
5.798	15	7.665	15	10.984	15	19.878	15	37.051	15
7.454	20	9.476	20	12.807	20	22.294	20	40.654	20
9.110	25	11.305	25	14.649	25	24.724	25	43.957	25
10.767	30	13.161	30	16.510	30	27.153	30	47.073	30

The relationship between shear stress and shear strain rate of sulfur composite at 140 °C

Several samples are measured at the shear strain rate of 1~60 1/s

20%									
F100		C25F75		C50F50		C75F25		C100	
τ (Pa)	γ̇ (1/s)	τ (Pa)	γ̇ (1/s)	τ (Pa)	γ̇ (1/s)	τ (Pa)	γ̇ (1/s)	τ (Pa)	γ̇ (1/s)
1.298	1	1.828	1	2.139	1	2.419	1	2.052	1
11.999	10	14.589	10	16.596	10	17.927	10	16.561	10
23.313	20	27.506	20	31.082	20	32.524	20	30.996	20
34.309	30	39.604	30	44.648	30	45.921	30	44.920	30
45.057	40	51.022	40	57.596	40	58.440	40	58.325	40
55.522	50	62.050	50	69.784	50	69.924	50	70.985	50
65.621	60	73.329	60	81.700	60	80.959	60	83.046	60
25%									
F100		C25F75		C50F50		C75F25		C100	
τ (Pa)	γ̇ (1/s)	τ (Pa)	γ̇ (1/s)	τ (Pa)	γ̇ (1/s)	τ (Pa)	γ̇ (1/s)	τ (Pa)	γ̇ (1/s)
2.249	1	3.246	1	3.616	1	4.332	1	6.238	1
10.030	5	22.298	10	21.028	10	2.516	5	19.350	5
18.969	10	41.523	20	37.341	20	2.022	10	32.162	10
27.578	15	59.895	30	52.455	30	1.799	15	43.750	15
36.856	20	77.481	40	66.850	40	1.653	20	54.251	20
45.265	25	94.113	50	80.660	50	1.558	25	64.361	25
53.417	30	110.905	60	94.308	60	1.484	30	73.876	30
30%									
F100		C25F75		C50F50		C75F25		C100	
τ (Pa)	γ̇ (1/s)	τ (Pa)	γ̇ (1/s)	τ (Pa)	γ̇ (1/s)	τ (Pa)	γ̇ (1/s)	τ (Pa)	γ̇ (1/s)
3.505	1	5.907	1	7.473	1	15.739	1	14.507	1
13.970	5	20.104	5	39.895	10	41.851	5	39.121	5
23.615	10	31.292	10	68.042	20	62.681	10	61.190	10
34.378	15	44.803	15	93.952	30	81.662	15	80.402	15
43.562	20	55.252	20	118.480	40	102.716	20	98.081	20
53.470	25	67.742	25	142.360	50	119.443	25	114.700	25
62.417	30	78.027	30	166.270	60	135.032	30	130.585	30
35%									
F100		C25F75		C50F50		C75F25		C100	
τ (Pa)	γ̇ (1/s)	τ (Pa)	γ̇ (1/s)	τ (Pa)	γ̇ (1/s)	τ (Pa)	γ̇ (1/s)	τ (Pa)	γ̇ (1/s)
5.746	1	9.494	1	24.668	1	22.133	1	28.964	1
21.590	5	36.069	5	60.002	5	65.298	5	86.563	5
39.290	10	65.298	10	93.034	10	104.125	10	141.862	10
55.017	15	93.239	15	123.480	15	138.020	15	177.391	15
69.919	20	119.465	20	156.659	20	168.855	20	220.821	20
82.354	25	141.800	25	179.733	25	197.570	25	262.110	25
93.490	30	162.330	30	201.176	30	225.180	30	301.682	30